International Forum on Aeroelasticity and Structural Dynamics
IFASD 2017
25-28 June 2017, Como - Italy

EXPERIMENTAL AND ANALYTICAL INVESTIGATIONS OF A FIGHTER-LIKE WIND TUNNEL MODEL WITH EXTERNAL STORES

Anders Karlsson [1] and Ulf Ringertz [2]

[1] Saab AB, Aeronautics,
SE-581 88, Linköping, Sweden
Anders.f.Karlsson@saabgroup.com

[2] Department of Aeronautical and Vehicle Engineering
Kungliga Tekniska Högskolan (KTH), Stockholm, Sweden
rzu@kth.se

Keywords: Aeroelasticity, flutter, limit-cycle oscillation, wind tunnel testing.

Abstract: In a recently finished project the ability to design and manufacture advanced wind tunnel models have been addressed as well as the development of tools for analysis of nonlinear aeroelastic phenomena. Experimental static tests of a real aircraft pylon-store test asset indicated a nonlinear behaviour in the sway brace and store interface for low preload cases. This characteristics was then replicated in a model scale with a detailed hardware realisation. A fairly extensive low speed wind tunnel program was performed with different store configurations as well as parameter variations of the sway brace preload and mass properties of the external stores. A failure case with a free-play between the wing tip missile and pylon was also investigated. Small differences were found in flutter speed and amplitude at the neutrally stable condition depending on the preload or introduced free-play. However, when the preload is reduced to half nominal value there was more of a constant amplitude (LCO) behaviour at the critical speed. This could be due to an amplitude dependent structural damping, something which numerically is shown to have a quenching effect.

1 INTRODUCTION

Current modern fighters continuously increase their capability to carry different external stores. Not seldom, the new stores are quite complex, both regarding the geometrical configuration with canards, wings, fins, multi-store carriers etc. and concerning the structural pylon interfaces with devices such as bomb racks and sway braces. This will increase the risk of encountering nonlinear phenomenon such as limit-cycle oscillation (LCO) due to aerodynamic and/or structural nonlinearities.
Therefore, there is a need in the industry to use nonlinear tools, also at early project stages with the objective to discover and assess the impact of phenomena such as LCO. However, when doing so, there is also a need for experimental validation and more understanding of the physical behaviour. In particular, results from aeroelastic wind tunnel tests are rare to find for complex geometrical configurations such as a fighter aircraft with external stores.

In the EDA project ISSA [1], with Italy and Sweden as main partners, one objective has been to increase the ability to perform nonlinear aeroelastic computations, focusing on fighter aircraft with external stores. The other objective has been to design, manufacture and perform wind tunnel tests of such a geometrically complex model in a cost effective way and to experimentally investigate the impact of structural nonlinearities on the aeroelastic

characteristics. Since the tests have been limited to the low speed wind tunnel at KTH, it has not been possible to account for all forms of aerodynamic nonlinearities in the experimental part of the project.

2 WIND TUNNEL MODEL

The aircraft geometry is characteristic of a modern light fighter featuring a closely coupled delta-wing canard configuration as shown in the left part of Figure 1. The basis for the design of the aeroelastic wind tunnel models used in the project are two models built around 1984 for flutter clearance testing. The configuration tested, shown to the right in Figure 1, did not include the canard but is otherwise representative of a modern fighter.

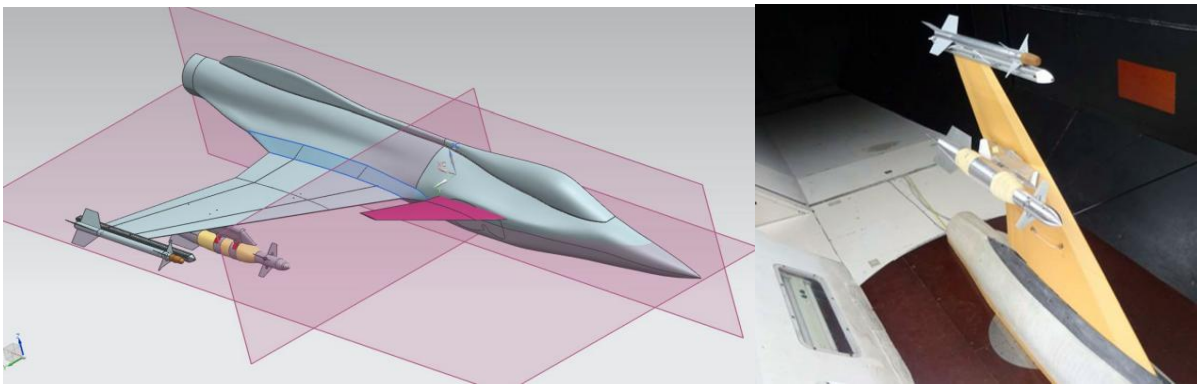

Figure 1: Conceptual design of the wind tunnel model and actual hardware in the tunnel test section.

2.1 Background

Since the wind tunnel testing in the current project was limited to low speed conditions, it was decided to investigate the possibilities of including some structural component with nonlinear characteristics that can be found on a real fighter aircraft. Therefore, in the early stages of the ISSA project, experimental static tests of a full scale aircraft pylon-store arrangement were performed. The results from this test indicated a nonlinear behaviour in the sway brace and store interface for low preload cases as shown in Figure 2.

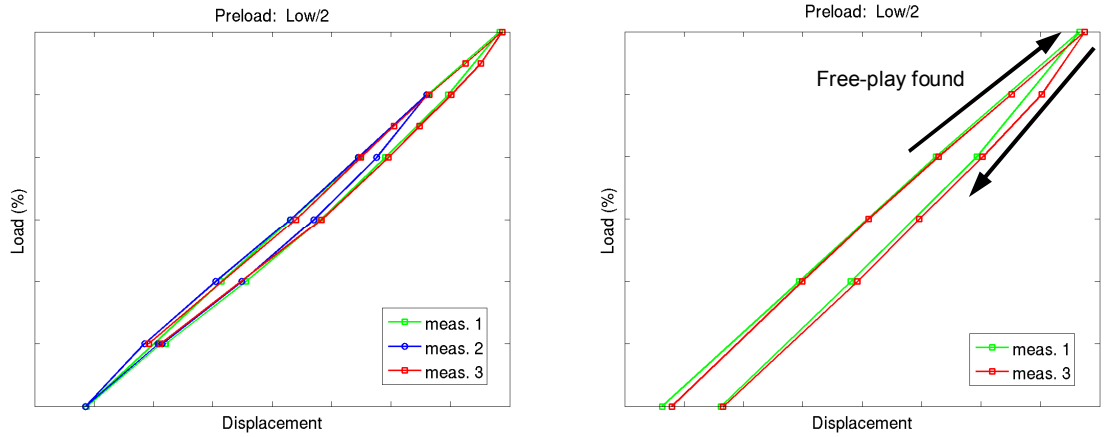

Figure 2: Measured static Load-Displacement characteristics of a full scale aircraft pylon-store arrangement.

This behaviour was found interesting enough to pursue by trying to replicate it in a model scale. The final model design of a pylon and sway brace is shown in Figure 3. The pylon housing is milled from a solid block of aluminium to ensure sufficient strength. It is attached

to the backbone of the wing via three bolts, two in the front and one in the rear part. Several different sway brace configurations have been investigated as can be seen from the lower part of Figure 3, with individual blades (variable number), single blade or stiff. The one chosen for the wind tunnel tests is the design with the four blade concept shown at the bottom left in Figure 3.

Figure 3: Model of pylon and sway brace. Load cells are measuring the preload.

In order to investigate whether the model has the same nonlinear characteristics as the full scale aircraft a test rig was used, see left part of Figure 4 for a schematic picture. The load versus displacement was measured where the loads were applied in the horizontal direction, both in tension and compression. The load cell data was obtained using a portable data acquisitions system [2]. Two separate runs were made with an applied external load in the ±70 Newton range. The load is changed by manually by turning the nut on a threaded bar which makes it somewhat difficult to make identical test runs.

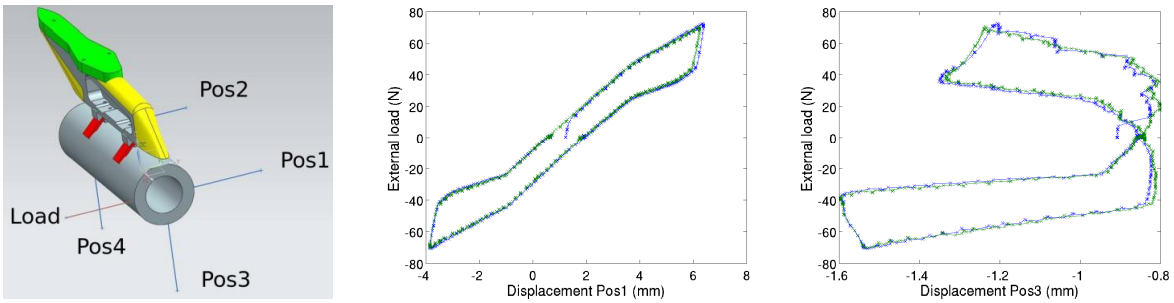

Figure 4: Static load measurements. Left: schematic picture of test rig. Middle: load vs horizontal displacement. Right: load vs vertical displacement.

As can be seen from the middle plot of Figure 4 a similar hysteresis was obtained for the model as in the full scale aircraft test for the measured horizontal displacement. A different hysteresis pattern was found for the vertical displacement where the deformation is also one order of magnitude smaller. Thus, a possible source to a nonlinear structural behaviour, as identified in the real A/C, could be designed and then measured in the model store/pylon interface. However, note that the dynamic properties and aeroelastic behaviour were unknown at the design stage and to be investigated in the wind tunnel tests.

As previously described, the current pylon design has a rigid housing as well as a stiff interface to the wing. A pre-study of a modified wing/pylon interface was also made but could not be realised within the budget of the project. Some kind of flexibility, allowing more lateral motion of the store relative to the wing, would have been desirable since this is occurring on the real aircraft due to flexibility of the housing. A flexible housing would be very difficult to implement in model scale though for this type of small scale project.

2.2 Wing Design

Most modern fighter wing structures are designed using carbon fibre reinforced composite materials to achieve sufficient stiffness and strength at low weight. These materials are not ideal for an aeroelastic wind tunnel model due to the high stiffness and comparably low failure strain. Further, a stressed skin structural design is difficult to achieve when designing for a low-speed wind tunnel because composite skins have to be extremely thin in order to ensure correct flexibility. Consequently, it is necessary to use different materials and construction techniques for the wind tunnel model. The present wing design consists of an inverse sandwich structure to give a correct outer aerodynamic shape and sufficiently low stiffness while simultaneously giving a strong backbone structure for attaching heavy external stores, control surface actuators and fasteners. The internal backbone structure, shown in Figure 5, consists of a fibreglass epoxy laminate which is cut to precise geometry using a waterjet cutting machine. The waterjet machine is computer controlled and is able to work from CAD geometry definition to give a final product with high geometrical precision. The fibreglass epoxy laminate is ideal for this application because of the moderate stiffness and very high failure strain. This material can consequently store a large amount of elastic energy since it can be deformed significantly without breaking or sustaining permanent damage.

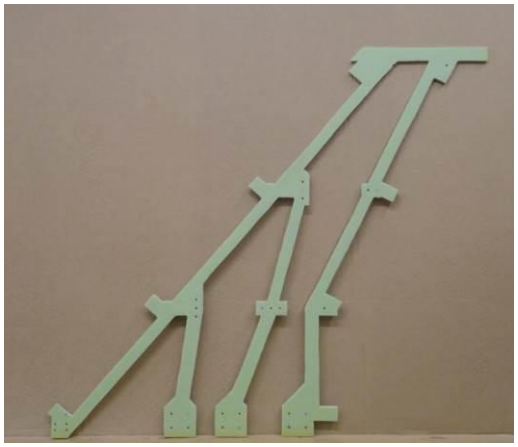

Figure 5: Internal fibreglass structure.

The aerodynamic shape is defined using an outer surface of a soft core material [3]. This particular core material is very suitable for flexible wing design as it behaves essentially linear and has a high failure strain and relatively low internal structural damping. The material is also available in different densities. For the current application, foam core densities of 130 and 200 kg/m^3 have been found suitable with sufficient surface smoothness and flexibility. The foam core material is cut using a computer controlled milling machine making it possible to manufacture core material parts with high precision at moderate cost. The foam core surface material is glued to the internal fibreglass structure using an epoxy resin with a slow curing process to ensure minimum shape distortion. Precise shape control in the assembly process is achieved using precision moulds as shown in Figure 6.

Figure 6: Moulds used for wing assembly.

2.3 Fuselage Design

The fuselage structure for the half model installation is designed using an internal support structure for the wing as shown in Figure 7. The fuselage shell does not carry loads from the lifting surfaces. This design makes it possible to change the wing support stiffness with limited modifications to the model hardware. The fuselage main spar is attached to the wind tunnel turntable making it possible to change the model angle of attack. The model is mounted on the wind tunnel floor in order to use the existing wind tunnel support structure. The fuselage design makes it possible to install a computer based data acquisition and control system inside the fuselage of the model. This way, it is possible to process measurement data inside the model which significantly reduces the amount of cabling that needs to be attached whenever the model is moved in and out of the tunnel test section. The data acquisition system uses a modular design making it possible to attach many different types of sensors to the system. A real time processor is used to analyse the data and convert analogue to digital information at high data rates. The data is then streamed to a host computer outside the tunnel test section using high speed Ethernet data communication.

Figure 7: Internal structure of the fuselage.

2.4 External Stores

The wind tunnel model can be equipped with a wing tip missile and an underwing store. The former is similar to AIM-9 and the latter resembles a GBU-16. The wing tip missile is attached to the wing using a launch rail similar to the design used on the full scale aircraft. The stores use a fairly stiff construction with aluminium or steel for all parts that carries significant loading during testing. An unique feature, developed at KTH, is that the external stores carries a movable mass in the form of a steel piston that can be moved during testing with compressed air or sub atmospheric pressures. Both store models have such a movable mass inside the external store which makes it possible to quickly change the structural dynamics of the wind tunnel model and saving the model in case of an aeroelastic instability.

2.4.1 Wing tip missile

The geometry is similar to, although not an exact scale model of, the common AIM-9 Sidewinder missile [4]. The missile is built up of a significant number of parts as shown in Figure 8.

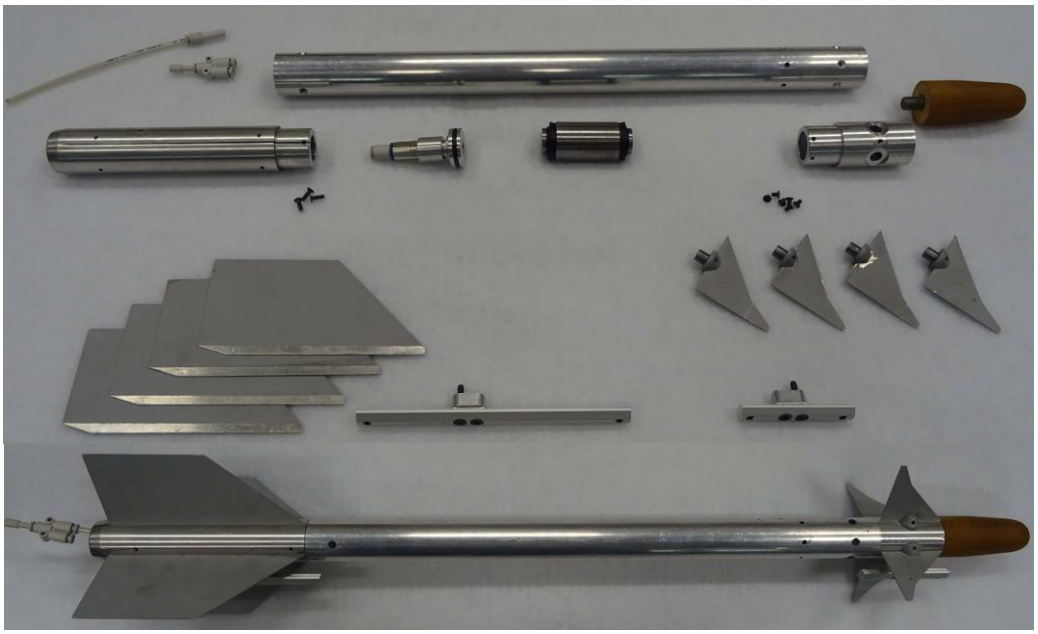

Figure 8: Wing tip missile parts (upper picture) and assembled (lower picture).

The modular design makes it possible to change mass distribution and aerodynamic fins may be removed or changed to a different geometry if desired. The movable steel piston is shown in the centre of the Figure and rubber seals are installed to increase efficiency of the pneumatic actuation system. A pressure tube is attached to the rear fuselage part. The tube is of small diameter (4 mm) so that it can be routed inside the wing to the pressure control system in the fuselage of the wind tunnel model. If the piston is in the rear position, compressed air can be applied rapidly moving the piston forward. The mass of the piston is significant, about 250 grams, in comparison to a total missile mass of 1 kg giving a rapid and significant change of structural dynamics and thus aeroelastic response. The missile is also defined in an accurate computer aided design (CAD) model shown in Figure 9. The CAD model is used as a geometry definition for generation of grids and meshes for computational fluid dynamics (CFD) analysis. The CAD model is also used for estimating inertial properties of the hardware. Mass and position of the centre of gravity can easily be measured but mass moments of inertia requires more difficult and less accurate dynamic testing. In the ISSA project, the geometry of each part is modelled in the CAD system and all corresponding parts are then weighed on a precision balance. The density of the material used for each part is afterwards adjusted so that each part has the correct mass in the CAD model. The CAD model can now be used to automatically compute all mass moments of inertia as well as the mass centre. This procedure has been found to be more accurate than trying to directly measure the mass moments of inertia. The missile is mounted on the launcher using slides in a rail slot on the launcher giving a mounting very similar to the one used on the real aircraft. The slide can be either clamped to the rail or blocked in the rail x-direction when free-play in the mounting is desired. The maximum total free-play is 0.2 mm normal to the wing and 0.48 mm in the wing plane (spanwise direction) resulting in a rotational play of about 6 degrees around the x-axis (streamwise direction). Since there are two slides, there will also be a free-play in the missile pitch rotation direction.

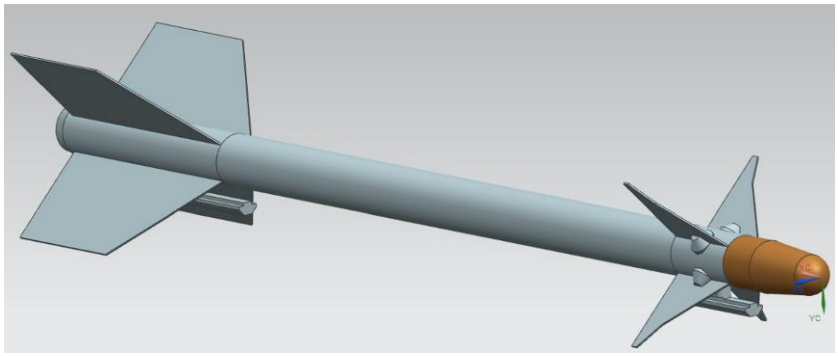

Figure 9: CAD model of wing tip missile.

2.4.2 Guided bomb unit

The external store mounted on the wing pylon is of the Guided Bomb Unit (GBU) type which is similar, but not built to exact model scale, to the Paveway II GBU-16 [5]. This external store is of particular interest as the aerodynamic lifting surfaces of the store could have significant impact on the aeroelastic characteristics of the aircraft. The parts making up the hardware as well as the assembled GBU for measurement of mass properties are shown in Figure 10.

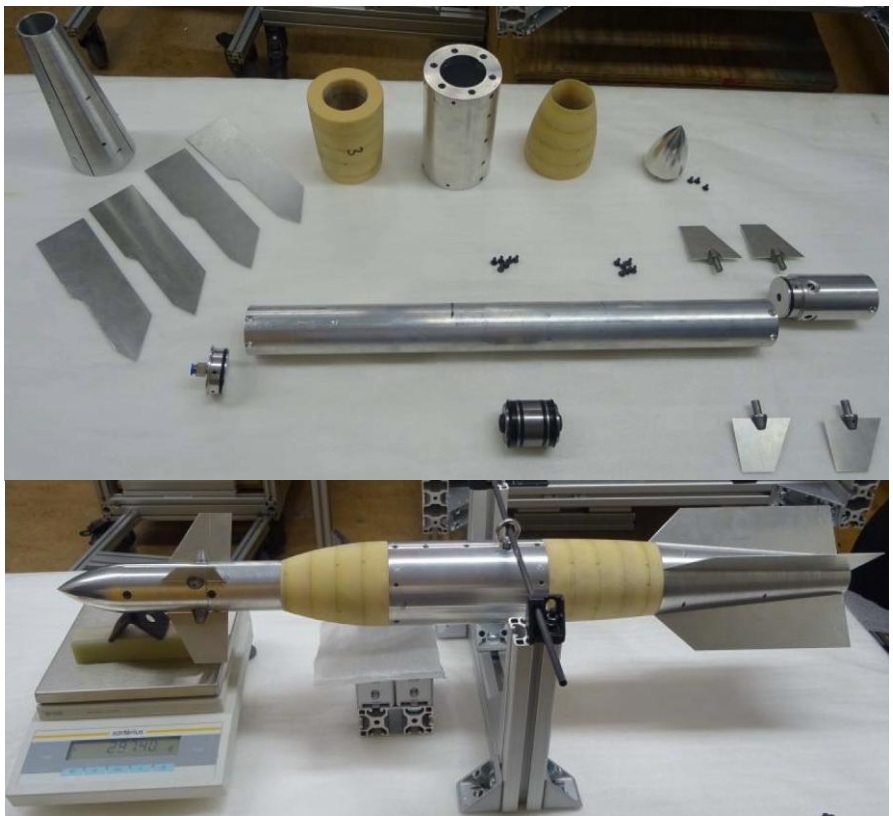

Figure 10: GBU parts and assembled GBU for measurement of mass properties.

3 NUMERICAL MODELS

For the analysis a number of different numerical models have been used. Both predictions of instability conditions and time domain simulations for estimating amplitudes at the LCO or neutrally stable conditions have been performed.

3.1 Linear analysis

The linear analyses have been performed mainly with DLM in MSC Nastran [6]. Also in-house tools have been used [7], [8]. The linear panel model for Nastran, shown in Figure 11, was in the ISSA project developed and verified by Leonardo Aircraft [9].

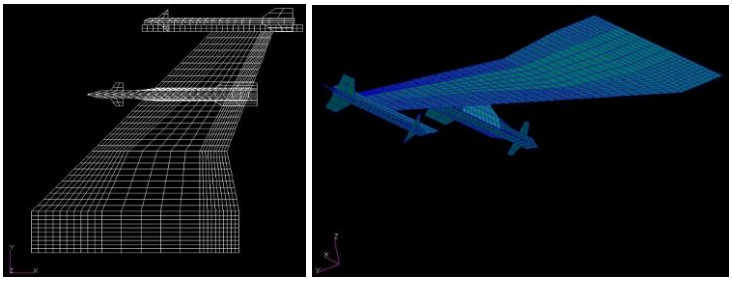

Figure 11: Linear DLM model used in MSC Nastran.

3.2 Nonlinear analysis

The nonlinear CFD-based analysis has been performed with the Edge code developed by FOI [10]-[12]. Edge is a parallelized CFD flow solver system for solving 2D/3D viscous/inviscid, compressible flow problems on unstructured grids with arbitrary elements. Edge can be used for both steady state and time accurate calculations including manoeuvres and aeroelastic simulations. Most computations presented in this paper have been based on a modal formulation for the equations of motion. Within the ISSA project, a new non-modal approach was also implemented by FOI which enables solving problems which are beyond the validity of the modal aeroelasticity such as nonlinear structure and or nonlinear deformations. A new time integration software, Extdyn, was developed for the computational structural mechanics working with NASTRAN to couple the two individual solvers. Special attention was paid to implementation of the communication scheme to the MPI version of Edge. Another aspect of current implementation is that it enables executing Edge in MPI mode on a cluster using cluster's submittal policy while running Extdyn on a different computer. The data communication process uses two utilities or libraries, libm3l and lsipdx [13], which enables proper and reliable synchronization and data exchange between two or more independently executed processes.

Although the non-modal approach has the potential of including structural nonlinearities this has not yet been exploited. In particular, the correct type structural nonlinear mechanism has to be identified and implemented, including detailed physical features such as friction, free-play, stiffness etc. For the test case used within ISSA, a friction type of structural nonlinearity was identified in the sway brace interface between the store and the pylon. This was investigated by other partners within the project (Politecnico di Milano) [14] using a very detailed (and time consuming) nonlinear structural model in ABAQUS. An alternative approach is to account for a local friction type of nonlinearity by a resulting global effect, e.g. as structural damping which increases with the amplitude. In [15] this was studied by Chen et al. for a case on the F-16 showing a quenching effect on the wing tip oscillation, going from an unstable to a LCO condition. A recent implementation in Edge has included a similar

feature with the possibility to give a structural damping which varies with the amplitude of a user specified coordinate.

All CFD-based flutter predictions are using the linearization concept where a small pulse perturbation according to (1) is used for excitation of each mode shape starting from the nonlinear steady state aerodynamics. The unsteady generalized aerodynamic forces are then computed from the quotient of the Fourier transforms of the force response and this pulse, see e.g. [16] for more details.

$$\delta_1(t) = \frac{1}{2}\left(1 - \cos\frac{2\pi\, t}{t_0}\right) \qquad \text{for } 0 \le t \le t_0 \text{ and 0 elsewhere} \tag{1}$$

Various computational meshes have been investigated, with the objective to obtain good enough convergence without having to resolve each physical detail that are of no importance for the global aerodynamic loads or local forces involved in the flutter mechanisms. As an example, for the most complex configuration the detailed geometry of the sway brace was, in most simulations, omitted since it deteriorated the convergence considerably both for the steady and unsteady computations. An example of such meshes is shown in Figure 12.

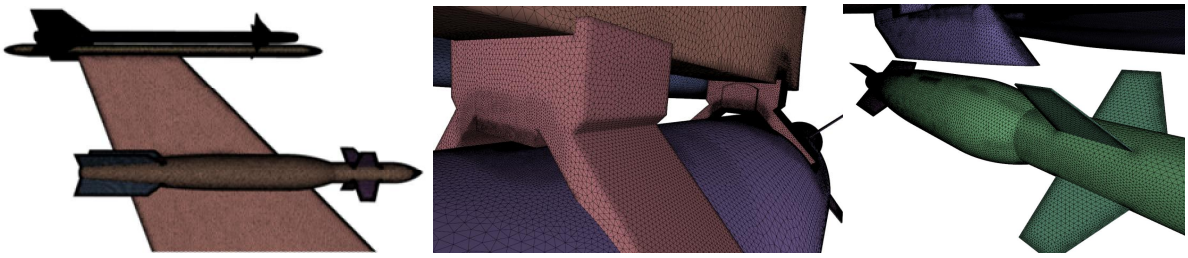

Figure 12: CFD meshes for Euler - including sway brace 4.3E6 grid points and without sway brace 2.6E6 points.

4 WIND TUNNEL CAMPAIGN

The wind tunnel program was fairly extensive and was carried out with different store configurations as well as parameter variations of the sway brace preload and CG positions of the external stores. Also a failure case with a free-play between the wing tip missile and pylon was included. Static deformation was measured for one configuration and dynamic data from accelerometers and an optical system [17] for deformation measurements were registered for all tested configurations. At subcritical speeds, excitation with a shaker was carried out in order to track modal parameters such as frequency as a function of speed. Testing was finally performed up to the critical speed for all the configurations, thus determining the flutter/LCO onset speed and frequency. The complete configuration test matrix is shown in Table 1. For all dynamic tests the angle of attack has been zero.

Configuration	Missile mass	Bomb mass	Static	Subcritical	Flutter
Clean wing	-	-	Yes	Yes	Yes
Wing tip missile	Rear	-	No	Yes	Yes
Wing tip missile	Forward	-	No	Yes	Yes
Tip missile and bomb	Rear	Rear	No	Yes	Yes
Tip missile and bomb	Forward	Rear	No	Yes	Yes
Tip missile and bomb	Rear	Forward	No	Yes	Yes
Tip missile and bomb	Forward	Forward	No	Yes	Yes

Table 1: Configurations tested in the wind tunnel trials.

Besides the wind tunnel trials, limited ground vibration testing (GVT) has also been conducted in close conjunction to the wind tunnel test (henceforth denoted WT-GVT). This, in addition to a more substantial GVT for validating and updating the FE model, prior to the wind tunnel tests (henceforth denoted FE-GVT). In both cases the model has been installed in the wind tunnel. For the WT-GVT the excitation was either manual or by shaker input at a span of frequencies. For oscillation controlled with shaker, excitation with a 32 seconds long chirp signal covering frequencies from 1 Hz to 8 Hz was applied to the wing structure. The frequency content in the structural response was determined either with accelerometer data or with data from an optical motion capture system. This WT-GVT turned out to be important since there was a difference in structural modal characteristics compared to the standard FE-GVT. In particular, a difference in frequency of the wing tip torsion mode was found with about 10% lower frequency in the WT-GVT compared to the FE-GVT. A possible explanation could be the various cables and accelerometer attachments used which were different for the two tests.

4.1 Instrumentation

Three types of accelerometers/sensors have been used; single axis accelerometers, 3-axis accelerometers and an optical measurement system. The wing is equipped with the smaller single axis accelerometers [18] to reduce aerodynamic interference. The pylon and the external store arrangements are equipped with 3-axis accelerometers [19]. The motion capture system [17] is used together with 4 to 7 markers placed on the upper side of the half span model for the GVT and dynamic aeroelastic testing. The positions of the accelerometers and markers are shown in Figure 13 with the single axis accelerometers (W) in the left figure, the 3-axis accelerometers (WT) in the middle figure and finally the optical markers (M) in the the right figure.

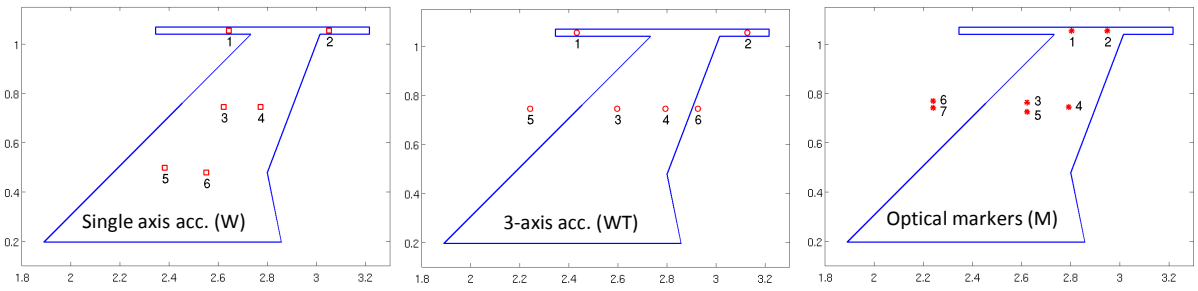

Figure 13: Location of accelerometers and optical markers.

5 WIND TUNNEL RESULTS

This paper will focus on results from the dynamic tests, presenting results such as instability speed and frequency, general dynamic characteristics and amplitudes at LCO-like conditions. Moreover, the amount of data is quite comprehensive so further confinements in the presented results are made with the emphasis on configurations including the GBU.

5.1 Critical Speeds and Flutter Mechanisms

In Table 2 results from the wind tunnel tests of the different configurations are shown. The results are sorted so that the lowest instability speed comes first and “fp” denotes a configuration including free-play for the wing tip missile. As can be seen, the most critical configurations are obtained for the case where the movable mass of the wing tip pylon is in

the rearward position which is an expected result and coincides with linear predictions. In fact, the characteristics is dominated by the position of the tip missile movable mass. Changing the movable mass position in the GBU has a minor, although not negligible effect.

Tip missile	Bomb	Name	Bomb sway braces	Velocity	Frequency
CG rearward	CG forward	MR_BF	4 blades,180 preload	38.9	3.4
CG rearward, fp	CG forward	MR_BF	4 blades,90 preload	38.9	3.4
CG rearward	CG forward	MR_BF	4 blades,90 preload	39.0	3.4
CG rearward	CG rearward	MR_BR	4 blades,90 preload	39.8	3.4
CG rearward	CG rearward	MR_BR	4 blades,180 preload	39.9	3.4
CG rearward	No	MR_0	-	41.4	3.9
CG forward	CG rearward	MF_BR	4 blades,90 preload	41.8	3.4
CG forward	CG rearward	MF_BR	4 blades,180 preload	42.2	3.3
CG forward	CG forward	MF_BF	4 blades,90 preload	42.4	3.3
CG forward	CG forward	MF_BF	4 blades,180 preload	42.5	3.3
CG forward	No	MF_0	-	43.0	3.7
No	No	0_0	-	44.2	6.0

Table 2: Critical speeds and frequencies at instability conditions for different hardware.

The flutter mechanism is a coupling between the two lowest modes, wing bending and wing torsion. The aeroelastic coupling is, however, different depending on configuration and thus not only dependent on the frequency quotient between these modes, see Table 3 for natural frequencies of the four lowest modes. This is illustrated in Figure 14, left plot, where the frequencies as a function of speed are plotted for both MR_BF (lowest predicted instability speed) and MF_BF (highest predicted instability speed). Although there is a smaller frequency separation at zero speed for the MF_BF configuration it is obvious that the aeroelastic coupling is stronger for configuration MR_BF. The effect of using an FE model tuned to the WT-GVT instead of the FE-GVT is shown in the right plot of Figure 14. The predicted flutter speed is lowered by approximately 2 m/s for the former case. When it comes to the mode shapes they are essentially identical for wing bending and wing torsion modes depending on the mass configuration but modes three and four differs somewhat depending on the position of the movable bomb mass.

Case	Mode 1	Mode 2	Mode 3	Mode 4
	Wing bend	Wind tip torsion	GBU pitch	Wing 2nd bend
MR_BF	2.20	4.28	7.40	8.95
MR_BR	2.14	4.48	7.30	8.74
MF_BR	2.20	4.38	7.48	8.54
MF_BF	2.26	4.24	7.28	8.99

Table 3: Natural frequencies from modal analysis of FE model tuned to FE-GVT.

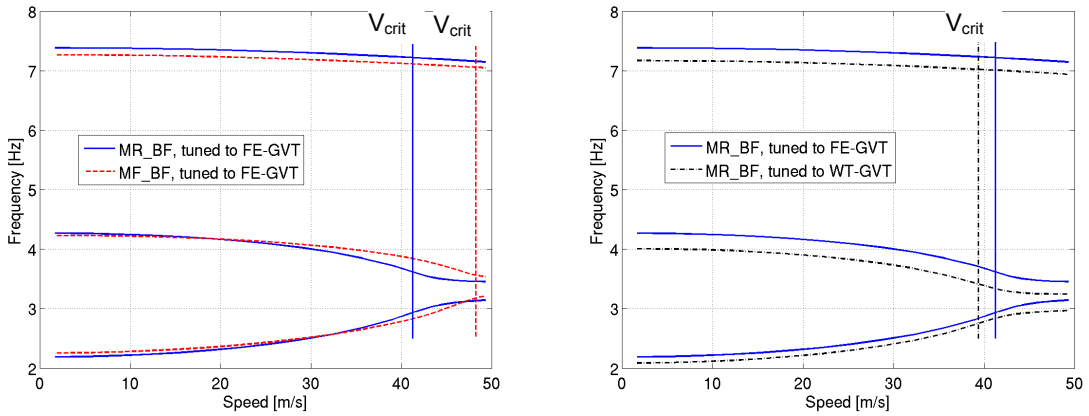

Figure 14: Results from Nastran - aeroelastic frequencies as a function of speed for conf. MR_BF and MF_BF.

As mentioned in Section 4, excitation with a shaker was carried out in order to track modal parameters at subcritical speeds. Therefore, experimental data such as the frequency is available and can be compared to the results from the analysis, see Figure 15. It can be seen that the predictions closely follow the experimental data when the FE model tuned to the WT-GVT is used. This also results in better predictions of the instability speed shown by the vertical lines in Figure 15.

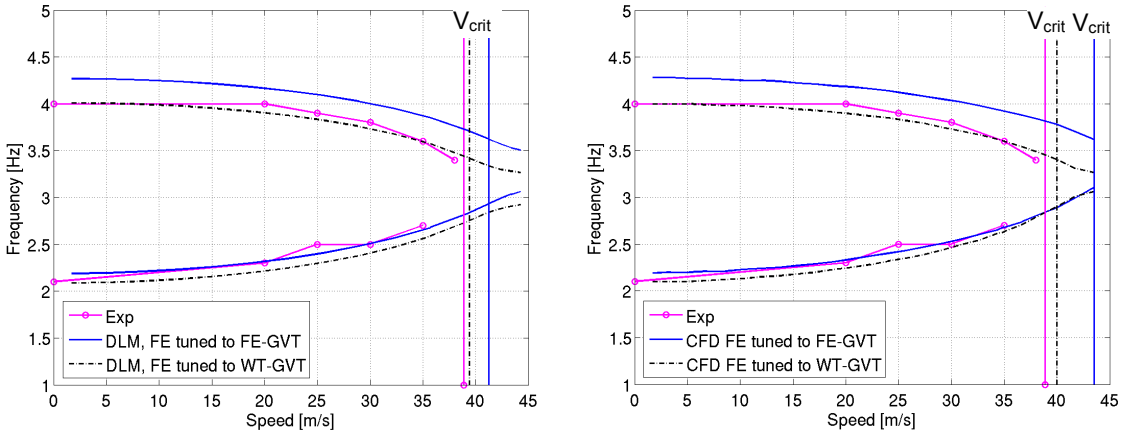

Figure 15: Results from Nastran/CFD - aeroelastic frequencies as a function of speed for conf. MR_BF.

5.2 Nonlinearities

In general, there seems to be a fairly small influence on the aeroelastic behaviour due to sources which can be related to structural nonlinearities. In particular, the results from the wind tunnel tests show a small impact on the instability onset speed and frequency depending on the sway brace preload, see Table 2. Also the free-play of the wing tip missile is rather insignificant, compare e.g. the three first lines in Table 2. The structural dynamics is as well essentially independent on the preload and free-play conditions as shown in Table 4. Slightly higher structural damping can be found for the bending mode (#1) when free-play is present.

Case	Preload	Mode 1		Mode 2		Mode 3	
		f	g	f	g	f	g
MR_BF	180N	2.13	1.5	4.02	1.7	6.97	1.5
MR_BF	90N	2.13	1.5	4.02	1.7	6.99	1.4
MR_BF	90N, free-play	2.11	3.4	4.01	1.6	6.93	1.4

Table 4: Natural frequencies, f [Hz] and structural damping, g [%] from WT-GVT.

However, there is one interesting observation found when studying the time histories of accelerometer data and comparing the amplitudes at the abortion (flutter) speed, as shown in Figure 16 for the MR_BF configuration. Here, one can see that for the case with the highest sway brace preload (180N) the amplitude is slowly increasing until abortion whereas for the case of half the preload (90N) the amplitude is quenched with a more or less constant amplitude oscillation.

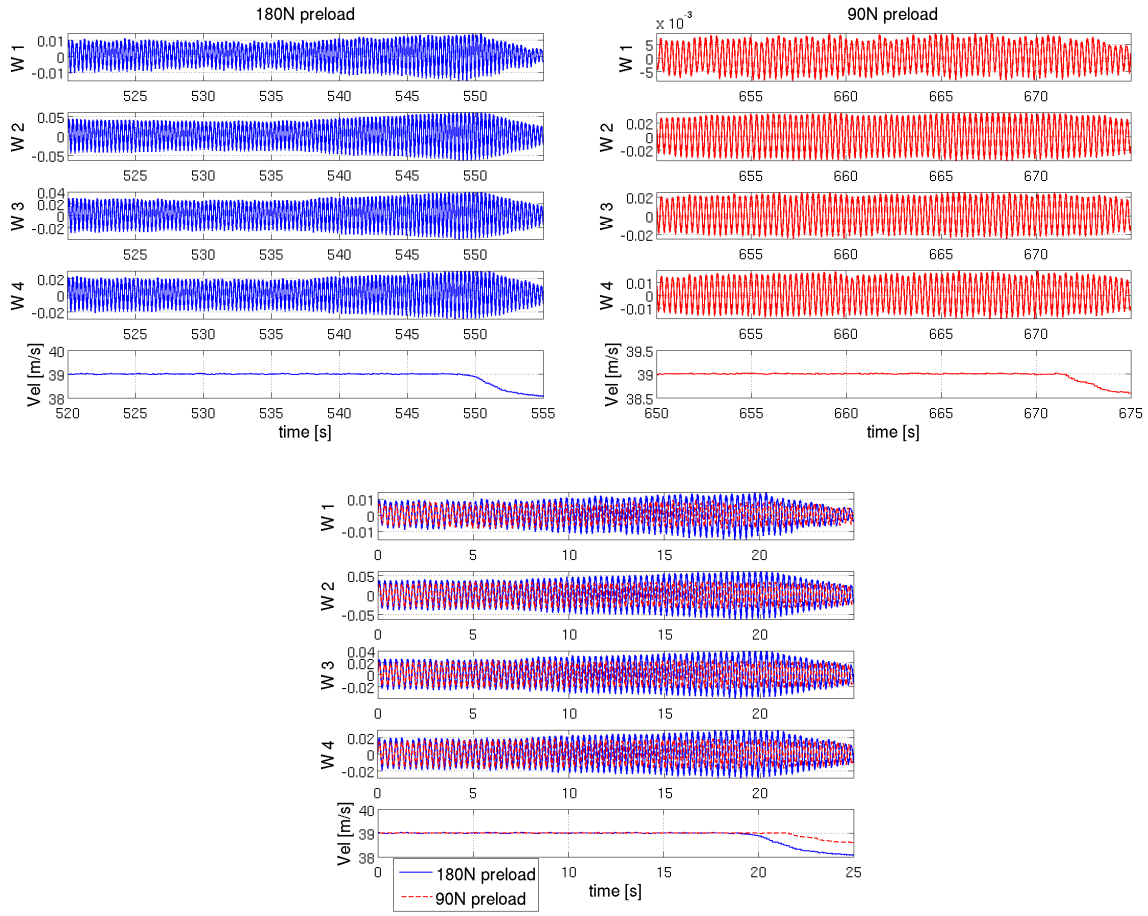

Figure 16: Accelerometer data just before abortion (instability condition). Blue 180N preload, red 90N preload.

A possible explanation for this could be that for the lower preload case there is more relative motion in the sway brace / store interface which then results in a structural damping that increases with the amplitude.

6 ANALYSIS RESULTS

Analytical predictions and simulations have been made with different tools including nonlinear aerodynamics where the CFD-based analyses have been limited to inviscid models based on the Euler equations. A fairly good agreement compared to the experiments for the flutter speed and frequency is obtained. However, the results have shown to be sensitive to input data such as having the exact representation mass and mass distribution which will affect the natural frequencies. In particular, as mentioned earlier the GVT updated FE model turned out to be slightly off for the torsion (and GBU pitch) mode. Therefore, results will be presented for different variants of the FE model, both tuned to the FE-GVT and to the WT-GVT.

6.1 Flutter Predictions

In Table 5 results such as critical speed (flutter/LCO) and corresponding frequency are presented for the most critical configuration, MR_BF, see Table 2. The analysis are based on different structural models, aerodynamic fidelity and model geometry. As pointed out above, the predicted critical speed is sensitive to the structural basis yielding a 5-7% lower critical speed using a structural model tuned to the WT-GVT which also correspond better to the experimental results. The CFD-based analysis actually yield a slightly higher predicted critical speed compared to the linear model and a small effect can be observed when accounting for the initial static deformation. Otherwise, the aerodynamic effect of the GBU bomb is small whereas the missile aerodynamics have a large influence on the predicted flutter characteristics. This is to be expected since the flutter mechanism is dominated by wing bending and torsion as previously shown.

Structural model	Aero model	CFD: V_{crit}	CFD: f_{crit}	DLM: V_{crit}	DLM: f_{crit}
FE-GVT tuned	complete	41.9	3.68	39.4	3.71
FE-GVT tuned + g	complete	43.5	3.58	41.2	3.62
WT-GVT tuned	complete	39.3	3.45	37.3	3.51
WT-GVT tuned + g	complete	40.7	3.37	39.4	3.42
WT-GVT tuned + g	complete + initial static def.	40.2	3.37		
WT-GVT tuned + g	no missile front wings			41.5	3.59
WT-GVT tuned + g	no missile wings or fins			40.8	3.52
WT-GVT tuned + g	No missile			43.8	3.52
WT-GVT tuned + g	No GBU wings or fins			39.4	3.43
WT-GVT tuned + g	No GBU	40.4	3.39	39.6	3.43
Experimental results		38.9	3.4	38.9	3.4

Table 5: Results from flutter predictions for configuration MR_BF.

6.2 Aeroelastic simulations

The results presented here are based modal based time domain simulations. When comparing amplitudes to experimental results the neutrally stable condition from the analysis has been taken (otherwise the amplitude is of no interest). However, note that for this type of low speed simulation, where no nonlinear structural quenching mechanism is included, the results are very sensitive to the initial transient applied. For the current results, an initial disturbance of mode 1, resulting in an initial total deformation slightly higher than the one obtained in the experiments, was used. Moreover, in order to have the most correct structural basis, the structural model tuned to the WT-GVT is used together with the measured structural damping from the FE-GVT.
Besides numerical uncertainties it is also important to highlight that the experimental results (amplitudes) vary within the exact same speed so the outcome of the comparison depend on the chosen experimental time segment.

A comparison of predicted (modal based) and measured amplitudes at the critical speed is shown in Figure 17 for the WT2 accelerometer and in Figure 18 for the W2 accelerometer. A first observation is that the two different types of accelerometers give a reasonable derived amplitude response (results are close with a larger amplitude further aft on the pylon). The analysis yield a predicted amplitude in the same order of magnitude and close in frequency but the outcome of the comparison is sensitive, both to the chosen experimental time segment and to the exact simulation condition including the initial transient perturbation.

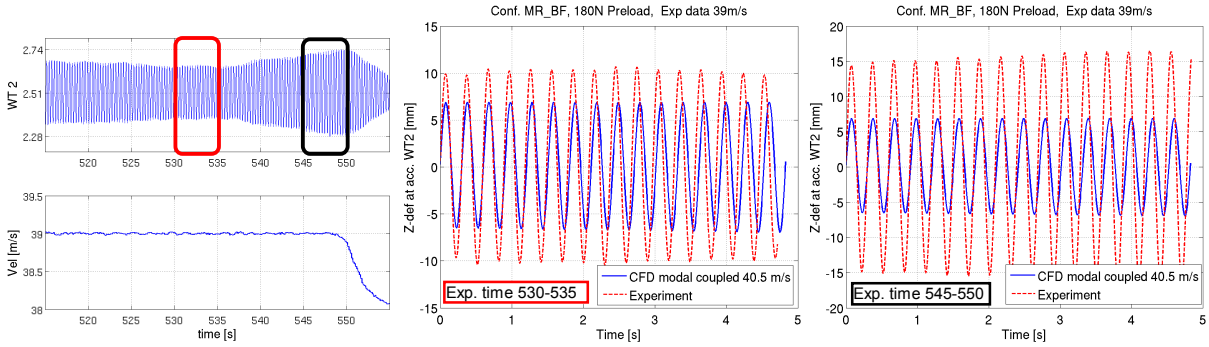

Figure 17: Measured (acc. WT2) and predicted amplitude for configuration MR_BF at the critical speed.

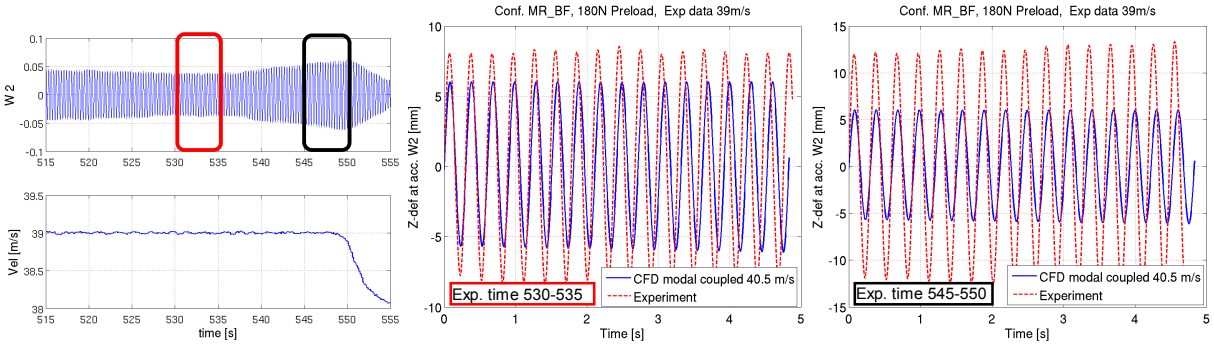

Figure 18: Measured (acc. W2) and predicted amplitude for configuration MR_BF at the critical speed.

When using accelerometer data the amplitude of the oscillation has to be derived from the acceleration and the frequency. An advantage of using the optical measurement system is that the deformation (position of the marker) is directly available. Example of results from the markers for configuration MR_BF at the critical speed, time segment 530-535, is shown in Figure 19.

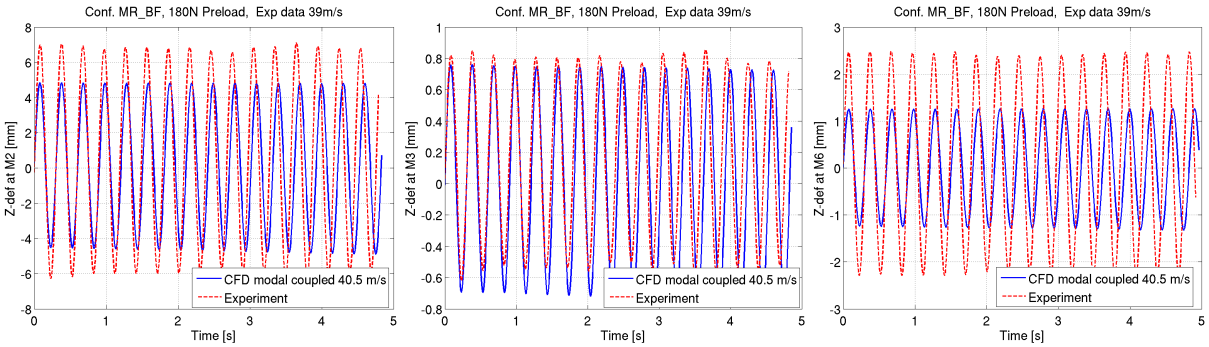

Figure 19: Measured (optical markers M) and predicted amplitude for configuration MR_BF at the critical speed.

Besides the uncertainties affecting the analysis mentioned previously, the configuration including the GBU will also have a deformation of the initial model shape due to gravitational forces. This mainly affects the static deformation but simulations also show a small effect on the amplitudes where analysis including gravitational forces yield slightly higher amplitudes. The influence on the stability predictions seems essentially negligible for the current case. The modal based results shown above are without gravitational forces.
In summary, more investigations need to be carried out for determining the best way forward when trying to estimate the amplitudes of dynamic simulations at the LCO / neutrally stable condition.

6.2.1 Nonlinear structural damping

Previously it was shown that for the lower preload case there was more of a LCO behaviour in the experimental results just before the critical speed. This could be due to a structural damping which is increasing with the amplitude. Unfortunately, at the time of the standard FE-GVT, the structural damping was not registered more than for one force level so there are no experimental data available. In order to illustrate the effect on the predicted amplitude when a nonlinear structural damping is used instead of a constant damping, simulations were made with Edge. Figure 20 shows a case where there is a weak instability if a constant structural damping (g) is used whereas more of a LCO condition is obtained when g increases with 25% for each doubling of the amplitude. A point at the rear part of the wing tip pylon was used as amplitude indicator for changing the structural damping.

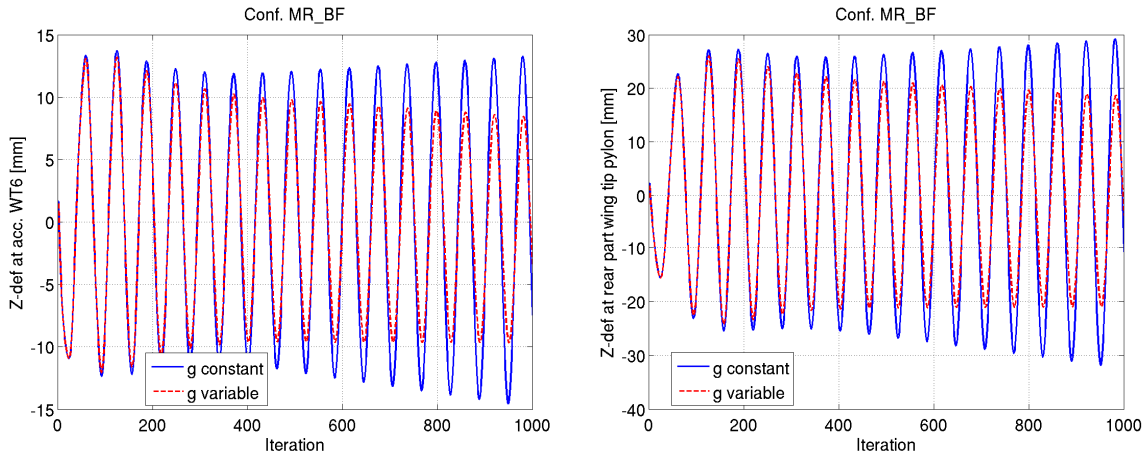

Figure 20: Time domain simulation with constant (blue) and amplitude dependent (red) structural damping.

7 CONCLUSIONS

It has been shown that it is possible design and manufacture advanced wind tunnel models, including a detailed hardware realisation of the pylon store interface, in a small scale project with a limited budget. The model pylon store interface could mimic characteristics to those measured on a real A/C test setup with nonlinear static behaviour for low preload cases. Low speed wind tunnel trials were performed for different store configurations, with a variation of the preload for the sway brace store interface as well as with a free-play in the wing tip missile rail attachment. The results from the wind tunnel campaign showed a small effect on the instability speed depending on sway brace preload or missile free-play. Also the modal characteristics, as measured in a GVT, were very similar depending on these parameters. It is possible that additional weakness in the pylon wing interface has to be introduced in order to allow more lateral motion of the underwing store and hereby obtaining larger relative motion between the pylon and the store. This, so that the nonlinear static characteristics found will appear also in the dynamic aeroelastic coupling. However, when studying the time histories of accelerometer data there was one observation which could be related to a nonlinear feature of the store and sway brace interface. At the instability speed, there was more of a constant amplitude (LCO) characteristics when preload was reduced to half the nominal value, something which could be due to an increased structural damping. Such a feature could also be demonstrated numerically.

8 ACKNOWLEDGEMENTS

The work within this study was a part of the EDA project ISSA. The Swedish part was financially supported by FMV, the Swedish Defence Material Administration where Curt Eidefeldt played an important role for enabling the project. The authors also would like to thank Adam Jirasek, Olivier Amoignon and Peter Eliasson (all former FOI) for the work with Edge, including mesh generation. Finally, David Eller at KTH has been contributing with ideas as well as geometrical models, meshes and support regarding the CFD/CSM coupling software.

9 REFERENCES

[1] EDA Contract No B 1190 ESM2 GP ISSA – ANNEX 1, "TECHNICAL PROPOSAL – Statement of Work For Integrated Simulation of Non-Linear Aero-Structural Phenomena Arising On Combat Aircraft In Transonic Flight".

[2] National Instruments. Operating instructions and specifications CompactRIO NI cRIO-9073, November 2011. www.ni.com.

[3] Divinycell H, Technical data sheet, February 2016, Diab Group, Laholm, Sweden, www.diabgroup.com/en-GB/Products-and-services/Core-Material/Divinycell-H

[4] Raytheon Corporation. AIM-9X Sidewinder, 2015. Data sheet, www.raytheon.com.

[5] Raytheon Corporation. Paveway Laser Guided Bomb, 2015. Data sheet, www.raytheon.com

[6] MSC Nastran, http://www.mscsoftware.com/product/msc-nastran

[7] V. J. Stark, "The AEREL Flutter Prediction System", ICAS-90-1.2.3, 1990

[8] Kuzmin et al., "Influence of Nonplanar Supersonic Interference on Aeroelastic Characteristics", International Forum on Aeroelasticity and Structural Dynamics, 1999.

[9] Marco Di Gifico and Vincenzo Vaccaro, "Improving Aeroelastic Model Accuracy and Affordability by Exploiting Wind Tunnel Test Results", International Forum on Aeroelasticity and Structural Dynamics, 2017

[10] Eliasson, P., "EDGE, a Navier-Stokes Solver for Unstructured Grids", FOI report, FOI-R-0298-SE, 2005

[11] Eliasson, P., "EDGE, a Navier-Stokes Solver for Unstructured Grids", Proceedings to Finite Volumes for Complex Applications III, 2002, pp. 527-534

[12] Eliasson, P., Weinerfelt, P., "Recent Applications of the Flow Solver Edge", Proceedings to 7th Asian CFD Conference, Bangalore, India, 2007.

[13] Adam Jirasek and Arthur W. Rizzi, "libm3l and lsipdx - Utilities for Inter-Process Data Transfer and Synchronization", AIAA paper 2014-1045, 52nd Aerospace Sciences Meeting, 2015

[14] A. Manes, A. Gilioli and M. Giglio, "An Investigation In Hi-Fi Finite Element Modelling Aimed To Improve LCO Prediction", International Forum on Aeroelasticity and Structural Dynamics, 2017

[15] P.C. Chen, Zhichao Zhang, Ayan Sengupta, and Danny D. Liu, "Studies of Limit-cycle-Oscillation Mechanism of Fighter With Stores Using an Euler With Boundary Layer Solver", International Forum on Aeroelasticity and Structural Dynamics, 2009

[16] A. Karlsson and B. Winzell, "Fluid-Structure Coupling With The Edge Program Applied to the Gripen Aircraft With Wing Tip Stores", International Forum on Aeroelasticity and Structural Dynamics, 2007

[17] Qualisys AB. Oqus - Qualisys motion capture camera with high-speed video. Product Information 100, 300 and 500 series, 2011.

[18] Kistler Instrument Corporation. Miniature PiezoBeam Accelerometer type 8640A, 2010. Data sheet, www.kistler.co

[19] Disynet. Disynet DA-series Kapazitive miniaturbeschleunigungsaufnehmer, January 2012. Data sheet, www.sensoren.de

COPYRIGHT STATEMENT